JOURNAL OF MATERIALS SCIENCE **38** (2003) 2105–2115

Single fibre deformation studies of poly(*p*-phenylene benzobisoxazole) fibres

Part II *Variation of crystal strain and crystallite orientation across the fibre*

R. J. DAVIES, M. A. MONTES-MORÁN
Manchester Materials Science Centre, UMIST/University of Manchester, Grosvenor St, Manchester M1 7HS, UK

C. RIEKEL
European Synchrotron Radiation Facility, B.P. 220, F-38043, Grenoble Cedex, France

R. J. YOUNG*
Manchester Materials Science Centre, UMIST/University of Manchester, Grosvenor St, Manchester M1 7HS, UK
E-mail: robert.young@umist.ac.uk

Changes in crystal strain and crystallite orientation of three varieties of PBO fibre (namely PBO AS, HM and HM+) have been investigated during deformation from the analysis of diffraction patterns obtained across single filaments, using a synchrotron X-ray source. Crystal strain was measured from the positions of the meridional reflections and orientation calculated from azimuthal broadening of the equatorial reflections. It has been demonstrated that no difference in crystal strain across the fibre exists, with the calculated strain being equal between fibre skin and core at a given level of stress. Further skin-core crystallite orientation analysis (calculation of the orientation parameter $\langle \sin^2 \theta \rangle$) proved that the AS fibre was the only PBO variety with a significant difference in orientation across the fibre, with the core region being less oriented due to the processing conditions. The skin and core orientation of all three fibres was found to improve with deformation, with the core of the AS fibre showing a significantly higher rate of improvement. This resulted in a similar level of orientation for both skin and core regions of the PBO AS fibre at high levels of stress. The fibre modulus was found to increase with the increasing initial degree of crystallite orientation. Furthermore, improvement in orientation with external stress was related to $\langle \sin^2 \theta \rangle_{\sigma=0}$, with higher values resulting in greater shear forces on the crystallites and therefore a greater rate of orientation improvement.

1. Introduction

This paper constitutes the second in a series examining single-fibre deformation of poly(*p*-phenylene benzobisoxazole), or PBO fibres, using synchrotron X-ray diffraction (XRD) studies [1]. PBO fibres are amongst a group of materials known as 'rigid-rod' polymer-based fibres due to their high degree of molecular chain conformation, and the rigid structure of their backbone repeat units:

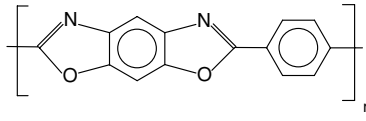

They are characterized by a high level of crystallinity and crystallite orientation, resulting in a remarkably high tensile strength and modulus compared to other high modulus polymeric fibres such as poly(*p*-phenylene terephthalamide) (PPTA). There are currently two varieties of PBO fibres commercially available, as-spun (AS) and high-modulus (HM). The AS and HM fibres are both manufactured using the same aqueous-based spinning technique, however the HM differs from the AS in that it receives a post-spinning heat treatment process which further improves the modulus of the fibre. A third fibre, ultra-high-modulus PBO (HM+), is currently under development, and is produced from a non-aqueous spinning process, resulting in a tensile modulus which is approximately 75% of the theoretical maximum value (or crystal modulus) [1–4].

* Author to whom all correspondence should be addressed.

Whereas the previous paper was concerned with examining the differences between the crystal modulus values of the three fibre types, and the relationship between crystal and tensile modulus [1], the present paper investigates differences in crystallite orientation and crystal strain *across* the fibre during deformation. Previous analyses of the crystallite orientation of PBO fibres can be divided into two aspects based upon the experimental method used. The first consists of orientation measurements across the fibre performed using selected area electron diffraction (SAED) studies [5–8]. SAED methods allow the determination of orientation from a specific point on the fibre, however the destructive nature of the required sample preparation means that it is then not possible to perform subsequent fibre deformation. The second comprises XRD experiments that examine overall orientation of the fibre, taken as an average of skin and core orientation [2, 4, 8, 9]. Using this approach it has been possible to determine the effect of loading on crystallite orientation, however the resolution has not enabled any 'skin-to-core' differences to be measured as fibre bundles were employed. Thus this publication will uniquely combine the benefits of both methods where the fine resolution using Synchrotron radiation is sufficient to enable skin-to-core orientation measurements, whilst simultaneous fibre deformation can also be carried out. This was achieved by using a micro-focus beam line (spot size of approx 3 μm) enabling diffraction patterns to be generated in steps across a single PBO filament (approx 12 μm of nominal diameter). This will therefore allow an investigation into the effect of deformation on these particular properties in relation to variations in processing between the three PBO fibre types. This will also provide information that may further explain the differences between the tensile and crystal modulus values reported in the preceding paper [1].

One of the aims of the present work is to establish possible differences in fibre morphology across a single PBO filament. As mentioned before, there have only been a limited number of previous studies examining such differences [5–8], related to the existence of a *skin-core* structure in PBO fibres. Such a skin-core structure is evident in numerous other fibres such as PPTA, and has been widely reported [10–14]. Before proceeding, a brief interpretation of the common terms *skin* and *core* will be given in the context of this work. As results presented here have been obtained from XRD patterns generated in transmission, it is only possible to achieve pure 'skin' diffraction patterns (where there is no additional 'core' diffraction) at the outer extremities of the fibre. For PBO, estimates as to the extent of the fibre 'skin' are in the range 10–200 nm [5, 8]. This therefore makes pure 'skin' diffraction impossible using the 3 μm beam diameter currently available as the amount of material in this region of the fibre would be insufficient to produce an accurate diffraction pattern. Bearing this in mind, the terms 'skin' and 'core' are used here purely descriptively for clarity and are not intended to imply that 'skin' refers to the specific fibre skin region. The term *skin* referred to herein is simply the morphological area described by the diffraction pattern furthest from the fibre centre, with *core* representing the diffraction pattern nearest the fibre centre. It must also be noted that any core diffraction obtained in such a way must also include a skin component through which the X-rays have passed. Ideally, it would be advantageous to deduct the skin diffraction from the core diffraction, in order to get a more accurate description of core morphology. However, as a consequence of the small skin thickness in the PBO fibre, it is not possible to calculate accurately the contributions of skin and core individually as pure skin diffraction is not available using this technique. Nevertheless, it is expected that the contribution of skin diffraction in the patterns generated is likely to be of little significance based upon the relative amount of core diffraction taking place.

2. Experimental

2.1. Materials

Three different types of PBO fibre, namely AS, HM and HM+ were investigated. The HM (high-modulus) fibres are produced commercially by Toyobo as Zylon®. The AS fibre corresponds to an as-spun PBO fibre, different from the commercially available Zylon®-AS. The PBO HM+ fibre is currently still in the development stage, although it is known that it was produced using a non-aqueous coagulation process, further details of which can be found elsewhere [2]. For the accurate determination of fibre diameters, a field-emission-gun scanning electron microscope (FEG-SEM) was used. Fibre diameters, tensile strength, tensile and crystal modulus are compiled in Table I [1].

2.2. X-ray diffraction (XRD)

XRD characterisation of the fibres was carried out at the European Synchrotron Radiation Facility (ESRF) on beamline ID13 (micro-focus beamline) [1]. The beamline was configured with the beam stopped down to a ~3 μm diameter spot size and a MARCCD detector. The specimen-to-film distance was calculated using an Al_2O_3 sample and was found to be approximately 68 mm. Further calculations were performed using the Al_2O_3 sample to determine sample rotation and tilt in order that these effects can be eliminated from the analysis. The fibres were loaded using a single-fibre stretching rig that was designed to fit to the x-y-z drive plate of the beamline stage. The deformation rig is based on a piezo stretching mechanism, and the load measured using an incorporated load cell. The gauge length between the mounting plates of the rig was 3.8 mm with a full deflection of 280 μm. Samples were glued using cyanoacrylate adhesive directly to the mounting

TABLE I Dimensions and mechanical properties of the three types of PBO fibre. (The figures in brackets are ±1 standard deviation)

	Fibre diameter (μm)	Strength (GPa)	Modulus (GPa)	Crystal modulus (GPa)
AS	12.3 (±1.1)	4.8 (±0.6)	180 (±10)	430 (±11)
HM	11.2 (±1.0)	5.5 (±0.7)	254 (±19)	474 (±7)
HM+	11.6 (±1.2)	5.4 (±0.9)	330 (±30)	454 (±1)

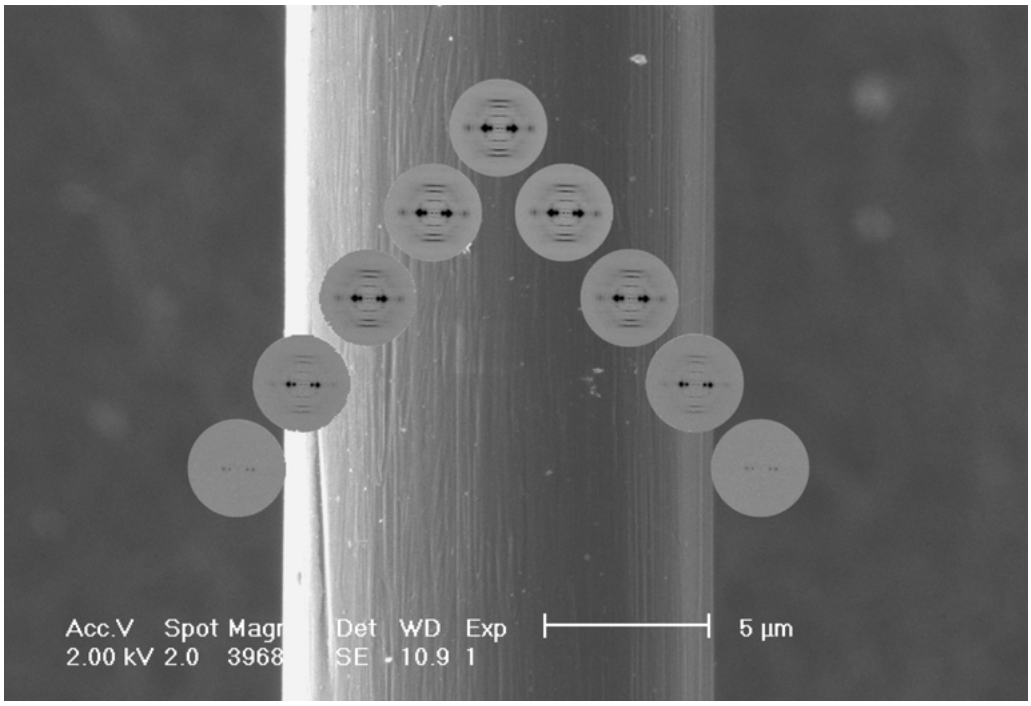

Figure 1 Diffraction patterns obtained across a PBO AS fibre superimposed upon a FEG-SEM micrograph indicating approximate beam width and position on fibre.

plates, and cured in situ prior to collection of data. Both the piezo mechanism and the recording of the load cell data were monitored from within the control cabin. Diffraction patterns were then generated using a 15 s scan time at $\sim$2 μm intervals across the fibre at increasing levels of loading, until either fibre fracture or debonding from the adhesive took place. This procedure was performed for all three of the PBO fibre varieties. Fig. 1 shows an example of the typical diffraction patterns generated across a single PBO HM fibre at zero load. In order to demonstrate the relationship between diffraction and fibre position, the diffraction patterns have been superimposed upon a FEG-SEM micrograph showing the approximate beam positions and diameter. (The diffraction patterns in Fig. 1 are displaced merely for clarity. The data were obtained in a line across the fibre diameter.)

For analysis of the diffraction patterns, all reflections were indexed after Fratini *et al.* [15]. The Fit2d software application version 10.95 [16, 17] was used to analyse and convert to appropriate formats the diffraction images produced. Another batch peak-fitting application was also custom written in Visual Basic for a more rapid analysis of the data, which is capable of calculating the orientation parameter $\langle \sin^2 \theta \rangle$ directly from azimuthal intensity data. This software is based on a modified Levenberg-Marquardt fitting algorithm, with integration of the results performed using the Romberg method. A more detailed account of the individual methods used to generate the orientation and crystal strain results are given below.

2.3. Crystal strain

The method used to calculate the variation of crystal strain across the fibre, was that performed in the first paper in this series [1]. However instead of using just the diffraction patterns generated from each fibre centre, patterns across the full fibre width were used. For each position on the fibre, the (005) and (006) meridional reflections were integrated in the radial direction above the beam centre. These particular reflections were chosen as they are particularly well defined, and are also a reasonable distance from the beam centre, thereby ensuring a sufficient movement of the reflections with deformation in order to calculate strain accurately. A pseudo-Voigtian function was fitted to the two reflections in order to determine their relative positions. The pseudo-Voigtian function was chosen as it was found to fit the data with the least number of residuals. Once this had been performed for one hemisphere of the diffraction pattern (the two reflections above beam centre for example), the same procedure was repeated for the opposite hemisphere. The resultant reflection positions could then be averaged for both the (005) and (006) reflections respectively. By doing this, any slight changes in beam centre position due to beam re-alignment would be cancelled out. One-dimensional diffraction grating theory was then used in order to calculate the c-spacing of the particular reflections [18]. Further details are found elsewhere [1].

2.4. Crystallite orientation

The (200), (010) and ($\bar{2}$ 10) equatorial reflections were chosen for the calculation of crystallite orientation because of their relatively high intensity and close proximity to the beam centre. Fig. 2 shows the central sections of PBO AS, HM and HM+ diffraction patterns from both fibres loaded to just below their failure stress and unloaded fibres for comparison. Initially, a radial slice of each diffraction pattern was analysed in order

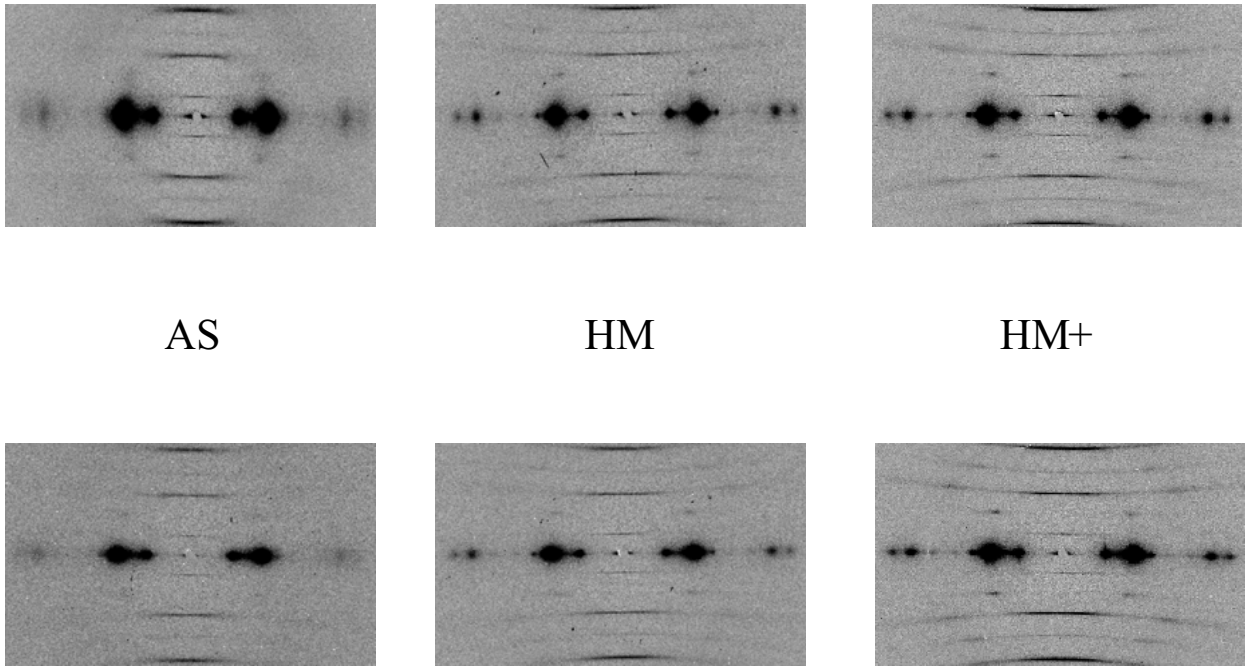

Figure 2 Diffraction patterns of single PBO AS, HM and HM+ fibres both unloaded (top) and loaded (bottom).

to determine the maximum radial position of each of the three reflections (Fig. 3a). These maximum points were then used in order to integrate the intensity of each reflection in the azimuthal direction. The integration was performed 180° around the peak maximum, as shown in Fig. 3b, with a total width value of 4 pixels. This value was chosen as a compromise between integrating enough pixels to produce an acceptable intensity profile, and avoid overlapping peaks or signal artefacts. The resultant intensity plots (Fig. 4) are therefore the azimuthal breadth of a given equatorial reflection, from –90° to +90°, 0° being the position of the equatorial peak's maximum azimuthal intensity.

In order to determine crystallite orientation, the well-known orientation parameter $\langle \sin^2 \theta \rangle$ was used [19–21]:

$$\langle \sin^2 \theta \rangle = \frac{\int_0^{\pi/2} \rho(\theta) \sin^3 \theta \, \mathrm{d}\theta}{\int_0^{\pi/2} \rho(\theta) \sin \theta \, \mathrm{d}\theta} \tag{1}$$

where $\rho(\theta)$ is the distribution of the orientation angle θ relative to the fibre axis, measured directly from the azimuthal spreading of the equatorial reflections. Therefore $\rho(\theta)\sin\theta \, \mathrm{d}\theta$ is the fraction of segments with an orientation angle between θ and $\theta + \mathrm{d}\theta$ [20]. To find the value of $\langle \sin^2 \theta \rangle$, the integrated intensity plots were fitted with a Lorentz-IV function [19] as shown in Fig. 4. This was in order to reduce the influence of background noise in the diffraction patterns at high angles (when the sine of the angle is close to unity). For perfect crystallite orientation $\langle \sin^2 \theta \rangle = 0$, i.e., the value of the crystal orientation parameter $\langle \sin^2 \theta \rangle$ decreases as the degree of crystallite orientation increases.

2.5. The weighted average technique

In order to derive an 'average' value which can be compared both more accurately with fibre bundle experiments, and also aid in the clarification of several aspects of the result analysis, an averaging procedure, weighted by gauge area, was also used for both the crystal strain and crystallite orientation results. Due to the shape of the beam irradiating area, which can be considered rectangular parallelepiped, gauge area averaged measurements are equivalent to gauge volume averaged ones since the depth contribution to gauge volume is proportional across the fibre.

The gauge area A_g was calculated for each diffraction pattern, based on the beam diameter, beam position and fibre diameter:

$$A_\mathrm{g} = 2 \times \int_l^u \sqrt{r^2 - x^2} \, \mathrm{d}x \tag{2}$$

where r is the radius of the fibre and x is the beam position integrated between the upper limit and lower limit, u and l respectively. The relationship between beamline geometry and gauge area is shown in Fig. 5.

The crystal strain and orientation results, at a given stress level, were then multiplied by the corresponding gauge area, and divided by the total area, thus producing the weighted average values:

$$Z_\mathrm{averaged} = \frac{\sum_n Z_\mathrm{n} \times A_\mathrm{g,n}}{\sum_n A_\mathrm{g,n}} \tag{3}$$

where Z_n is the value of the particular property (crystal strain or orientation parameter) calculated at position n on the fibre, and $A_\mathrm{g,n}$ is the gauge area for the n beam position. Therefore, a value obtained from a diffraction pattern in the centre of the fibre would influence the result to a greater degree than a diffraction pattern from the fibre extremities, due to the greater amount of material in the beam.

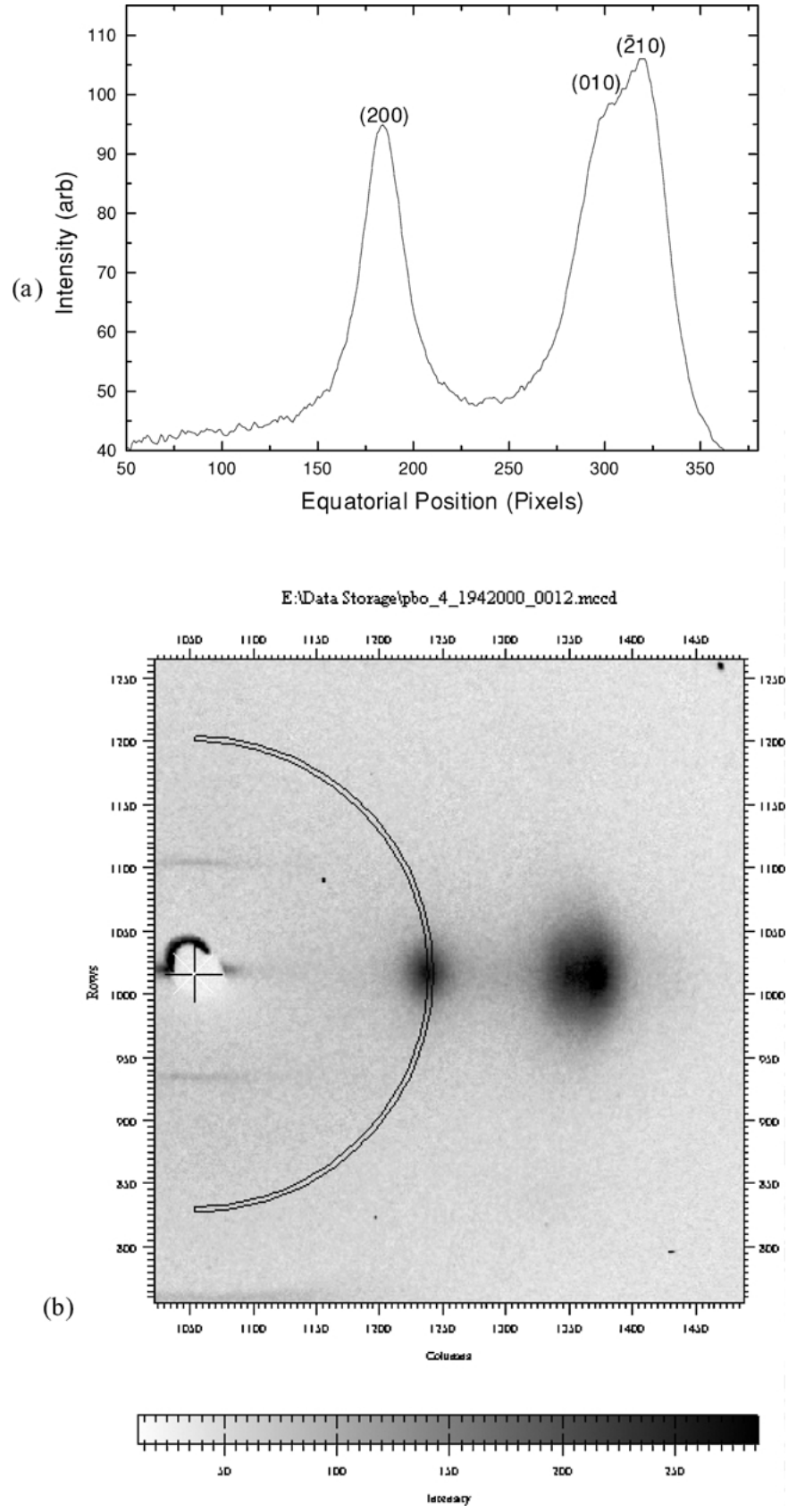

Figure 3 (a) Radial intensity profile of the PBO equatorial main reflections, and (b) example of azimuthal 'cake slice' on the (200) reflection of PBO AS.

3. Results and discussion

The results have been divided based upon the fibre property being examined, namely crystal strain and crystallite orientation. Both of these properties have then been sub-divided in order that clarity and coherency is maintained throughout the discussion. Firstly, differences between the morphology across the fibre with deformation will be considered. Secondly, the weighted average values will be discussed in order to identify the influence of deformation on the overall crystal strain and orientation of the PBO fibre types, to be consistent with previous fibre bundle studies.

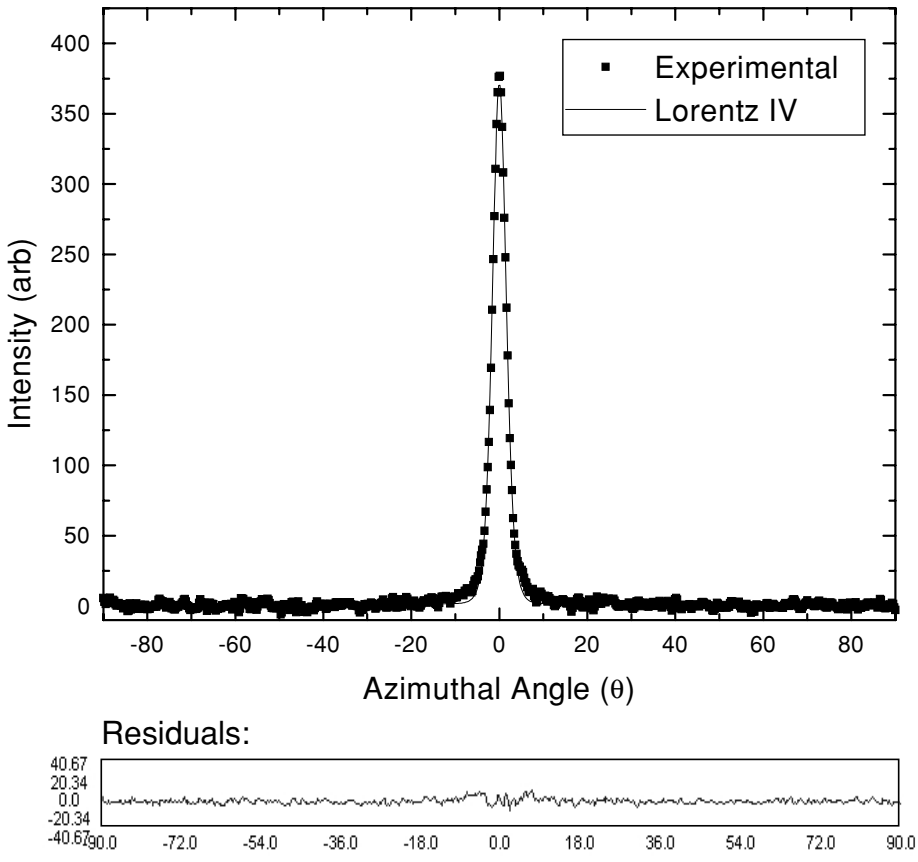

Figure 4 Demonstration of the intensity of the azimuthally integrated (200) reflection with angle of PBO AS and subsequent peak fitting. (The residuals plot shows the difference in intensity between the measured data and fitted curve).

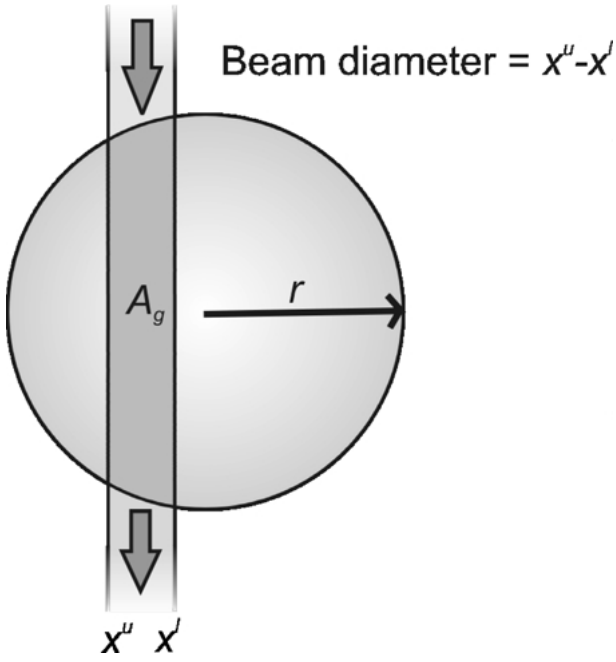

Figure 5 Calculation of fibre gauge area based upon beamline geometry.

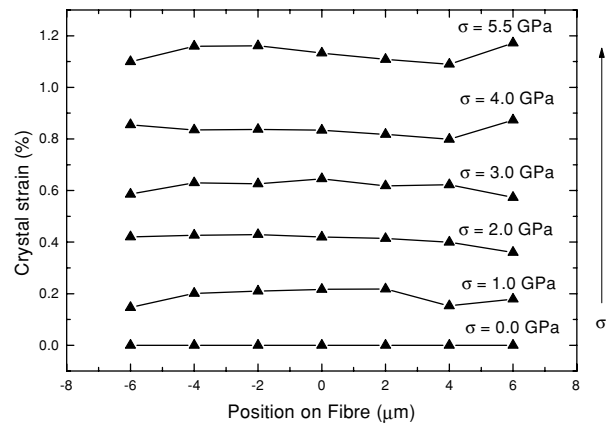

Figure 6 Crystal strain variations across a single PBO HM fibre with increasing stress.

3.1. Crystal strain

3.1.1. Differences across the fibre

The crystal strain across the fibre can be determined by using the procedure of measuring meridional peak position from diffraction patterns taken across the fibre during deformation. Fig. 6 shows the crystal strain plots across the fibre for the PBO HM fibre. The plot indicates that there exists a uniform crystal strain between fibre skin and fibre core, with no obvious skin-core differences in crystal strain during deformation. A similar result was also found for the AS and HM+ fibres, both of which also exhibited uniform crystal strain, and are therefore not shown. This is, to the authors' knowledge, the first time variations in crystal strain across PBO fibres during deformation have been investigated using XRD.

3.1.2. Averaged values weighted by area

It has already been demonstrated that during deformation, there are differences in the crystal strain responses

to an applied stress between the three PBO fibre types resulting in different crystal modulus values [1]. These results from the previous paper are shown in Table I. As also discussed in the first paper in this series [1], the crystal modulus values of the various types of PBO fibre have been determined by several groups using fibre bundles [2–4]. This bundle method provides an average value of crystal strain during fibre deformation, based upon an assumption of homogeneous stress [1]. As mentioned in the Experimental section the use of averaged values weighted by area should, in principle, provide results more comparable to those obtained with fibre bundle experiments.

Fig. 7 shows a comparison of the weighted average crystal strain plotted against applied stress for the three PBO fibre varieties, with the corresponding crystal modulus values. Again the PBO HM fibre demonstrates the highest crystal modulus value, with the HM and HM+ fibres having lower values. These values agree reasonably with those of previous studies [2–4, 22]. It is worth pointing out that the results obtained from averaging the skin-core crystal modulus values are only slightly different from those calculated in the preceding paper in this series when only the core regions were used in the calculation (Table I) [1]. This is to be expected, since crystal strain has been shown to be uniform across the fibre (Fig. 6). Any slight differences between the results are caused by averaging crystal strain across the fibre, therefore leading to a reduction in the significance of background noise and artefacts. This is demonstrated by comparing the significantly lower scatter of data shown in Fig. 7 when compared to similar plots appearing in the previous paper [1].

The crystal modulus value of the HM+ fibre was found to be similar to that determined recently by Kitagawa and Yabuki of 460 GPa [4]. This is significant as that value had not yet been reported during preparation of the last paper in this series [1]. This further indicates that the assumption of homogeneous stress, necessary for fibre bundle diffraction, is valid in the case of PBO.

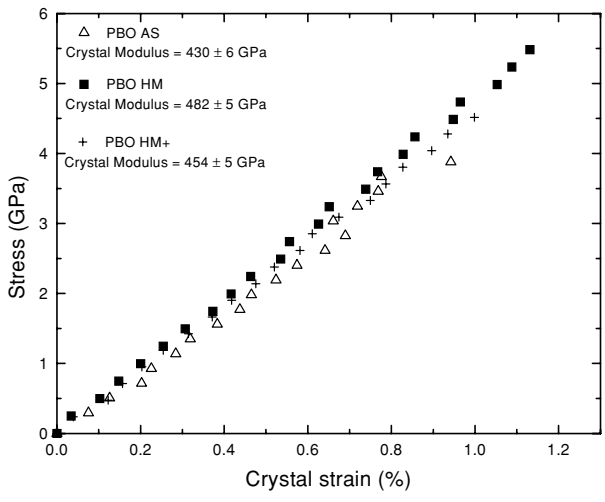

Figure 7 Variation of weighted average crystal strain with applied stress and resultant crystal modulus values of PBO AS, HM and HM+.

3.2. Crystallite orientation

3.2.1. Choice of equatorial reflection

Before discussing the results obtained for orientation across the PBO fibre, a brief explanation will be given on the choice of equatorial reflection when using this method to determine orientation. Crystallite orientation analysis was performed on the (200), (010) and ($\bar{2}$ 10) reflections, in order to assess the influence of equatorial peak choice on the results obtained. It was found that the choice of equatorial peak did indeed strongly influence the orientation results obtained. The overall 'weighted average' orientation level at any given stress was found to be dependent upon the equatorial peak employed, with the (200) reflection giving the lowest orientation parameter in all cases. Both the (010) and ($\bar{2}$ 10) reflections returned a higher value of orientation parameter for all fibre types. However, the rate of change of orientation with stress was the same regardless of equatorial reflection used.

In terms of orientation analysis across the fibre, it was found that no significant difference between the skin and core orientation existed in the AS, HM or HM+ fibres using either the (010) or ($\bar{2}$ 10) equatorial reflections, contrary to the results obtained using the (200) reflection. The reason for these differences may be the proximity of the (010) and ($\bar{2}$ 10) reflections to one another, and their distance from beam centre. The (010) and ($\bar{2}$ 10) reflections are so close that accurate determination of the intensity of one reflection is difficult without some intensity overlap from the adjoining reflection, as shown in the radial integration in Fig. 3a. Also, as the azimuthal breadth will increase proportionally with the distance from beam centre, the intensity profile becomes more dispersed, thus background noise will increasingly influence the results. It is also possible such differences could be attributed to the measurement of orientation using different crystallographic planes. Due to the radial texturing of fibrils within the fibre, and the non-primitive monoclinic structure of the PBO unit cell, the choice of reflection would be expected to influence the results to some degree.

Previous publications which include a quantifiable orientation analysis have been performed using the (200) reflection and this provides a sound basis for comparison with this work [2, 4, 8]. This has been chosen presumably because of the high intensity of the reflection, its proximity to the beam centre and the aforementioned intensity 'overlap' of the alternatives. Similar studies with other highly oriented fibres such as PPTA have also used (200) as an isolated equatorial reflection in calculating orientation [19, 21].

It is therefore clear that the (200) reflection is the only PBO equatorial reflection that can be used to accurately determine skin-to-core orientation differences using this method and is also the reflection that returns the lowest value of the orientation parameter.

3.2.2. Differences across the fibre

Fig. 8a, b and c show crystallite orientation across the fibre for the PBO AS, HM and HM+ fibres at different stress levels. In the undeformed state, the PBO AS

and HM+ fibres both show a considerable difference in orientation parameter with fibre position, this being lower in the fibre core region and then increasing with distance. This is also true of the PBO HM fibre, although in this case the difference in orientation between skin and core is marginal. Although, as mentioned previously, it is not possible to measure pure 'skin' diffraction quantitatively, it is quite clear from the results that the fibre skin regions would show the greatest degree of crystallite orientation (lowest value of $\langle \sin^2 \theta \rangle$). SAED investigations on the same type of fibres [5, 6] have also shown similar results, with fibres demonstrating a greater orientation in the skin crystallites compared to that in the core region, consistent with other highly-oriented fibres such as PPTA [10–14]. This has been attributed to the shear forces generated

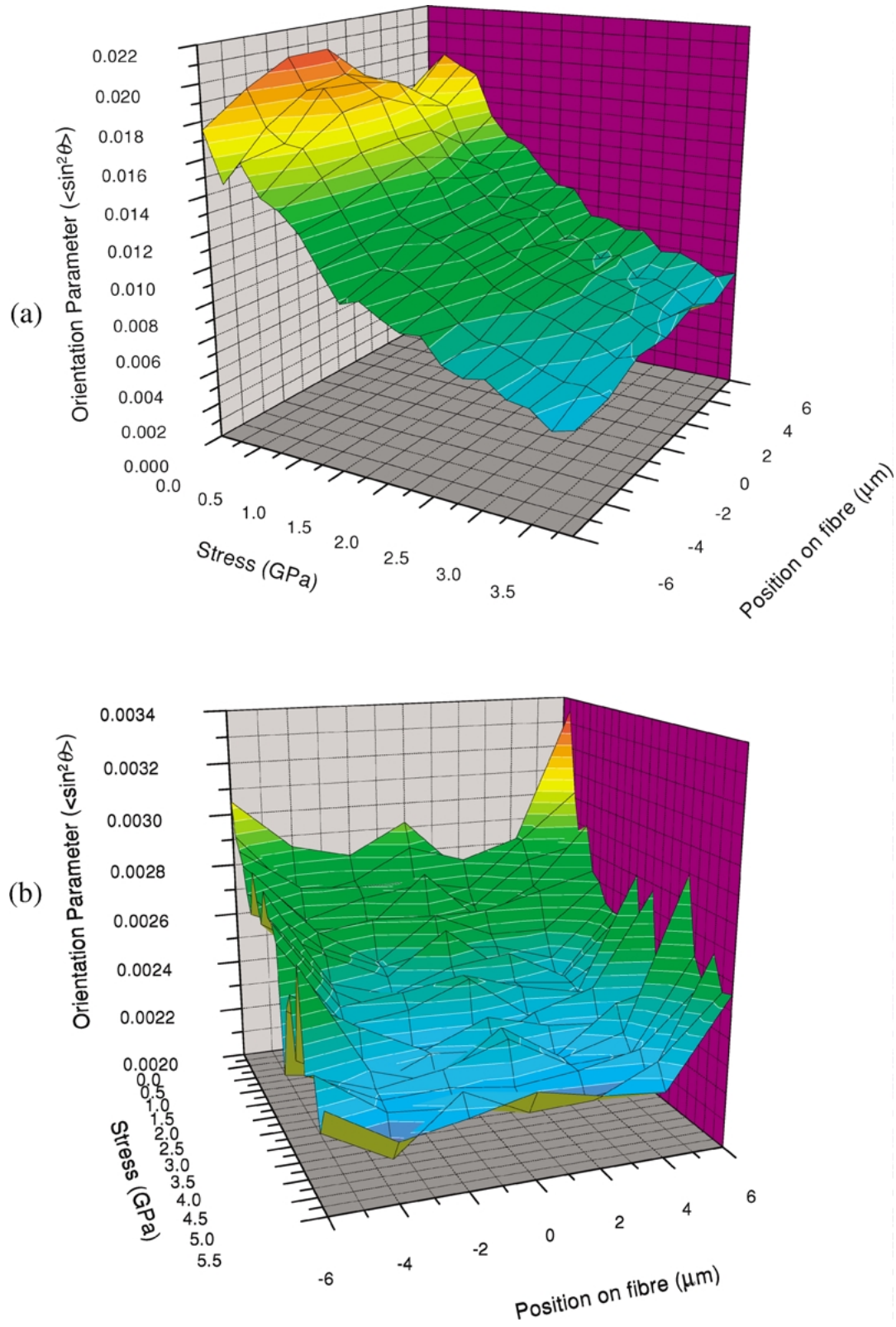

Figure 8 (a) PBO AS crystallite orientation parameter across fibre with stress, (b) PBO HM crystallite orientation parameter across fibre with stress, and (c) PBO HM+ crystallite orientation parameter across fibre with stress. (*Continued*)

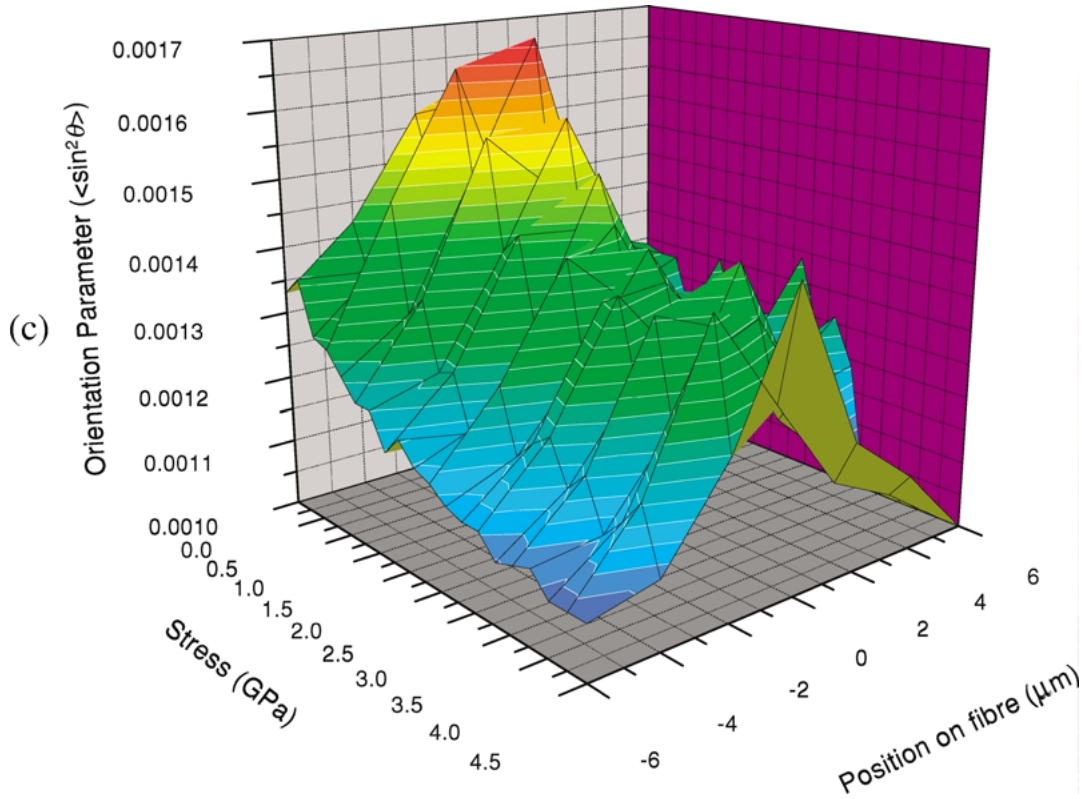

Figure 8 (*Continued*).

during the spinning process which increases alignment of the skin crystallites to the fibre directional axis [12]. Young *et al.* [6] have reported a significant reduction of the skin-core feature when comparing PBO AS and HM fibres. It is believed that the heat treatment process has been responsible for increasing not only the crystallite orientation of the PBO HM fibre, but also for reducing the initial skin-to-core orientation observed in the as spun fibres.

Recently, Kitagawa *et al.* [7] published a comparison of skin-to-core orientation which also included the HM+ fibre type, again using a SAED technique. Contrary to previous XRD studies [2, 4], there was found to be little structural difference between the AS and HM fibres, although the HM+ fibre had a greater difference in orientation between skin and core [7]. Although the average degree of orientation of the crystallites measured using SAED increased proportionally the same amount as that found using XRD [2, 4, 7], the actual skin-to-core orientation calculations showed that differences in the orientation values for the three fibres were inconsistent with XRD studies. Whilst the higher orientation parameter $\langle \sin^2 \theta \rangle$ values obtained overall may be attributed to electron beam broadening and changes in scanning intensity [7], these factors cannot explain the relative differences between the measured crystallite orientations. The skin-to-core orientation measured using SAED shows all three fibres to have a similar difference in orientation to one another [7]. This might indicate that there are other influences that have not been accounted for such as possible structural modification of the samples during sectioning which could be affecting the results.

It should be noted that the scales of the orientation parameter axes are different on each plot in Fig. 8a, b and c, making a direct comparison of the three fibre types difficult. Fig. 9 shows a single plot with all three fibre types for comparison, where four similar stress levels are plotted for each fibre as labelled for the AS fibre for reference. In such a direct comparison, it can be observed that there is no significant skin-core orientation in either the PBO HM or PBO HM+ fibres, indicating that the heat treatment process significantly reduces this effect as has been previously reported [6].

During deformation, there are two main aspects that should be discussed. Firstly, all three fibres show an improvement in orientation in both the fibre skin and fibre core regions, with the increase being related to the degree of initial orientation. This subject can be more conveniently discussed in terms of averaged orientation values (see next section). Secondly, it can be observed that the AS fibre has a much greater

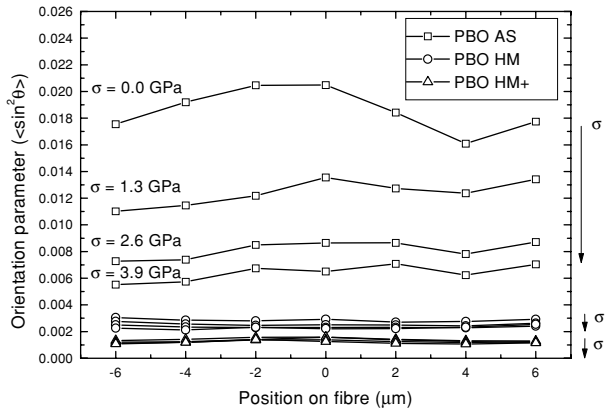

Figure 9 Comparison of crystallite orientation across fibre for all fibre types at four different stress levels.

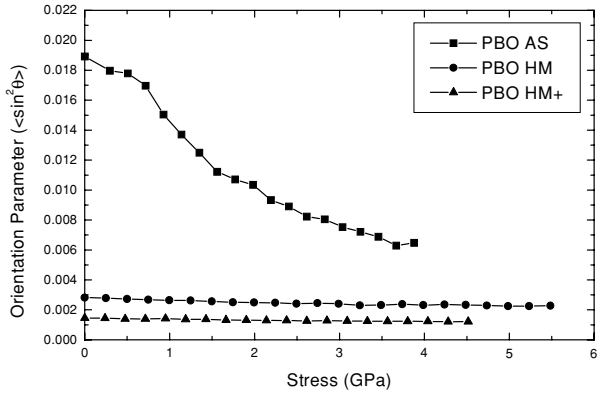

Figure 10 Variation of weighted average crystallite orientation parameter with applied stress.

improvement in the core orientation than in the skin region, so that at high levels of applied stress, the core and skin show approximately the same level of crystallite orientation.

3.2.3. Averaged values weighted by area

Fig. 10 shows the average weighted crystallite orientation values against applied stress for all three PBO fibre types. It can be seen that initially, with no deformation occurring, the AS fibre is significantly less well oriented than both the HM and HM+ fibres, with the HM+ fibre being slightly more oriented than the HM fibre. As mentioned above, several previous studies have shown that the AS fibre has a poorer orientation than the HM fibre, thus indicating that it is the heat-treatment process which significantly improves the orientation [2, 4–9]. Further reduction of the observed $\langle \sin^2 \theta \rangle$ values for the PBO HM and PBO HM+ can be possibly linked to differences in the processing route, most significantly the use of non-aqueous spinning solution aimed to reduce the density of flaws [4].

Most previous studies have not determined orientation quantitatively, and thus only the order of orientation can be compared [5, 6, 9]. Few of them [2, 4, 7, 8], however, actually calculate values of $\langle \sin^2 \theta \rangle$ for different types of PBO fibre. These results are collected in Table II, as well as those obtained in the present work. Apart from differences arising when SAED or XRD generated values are compared (which has already been discussed in the previous section), very different $\langle \sin^2 \theta \rangle$ values can be observed even when they are obtained from the same experimental method. For example, XRD results reported by Kitagawa *et al*. show a lower degree of orientation by more than a factor of two in $\langle \sin^2 \theta \rangle$ for the HM and HM+ varieties when compared to our results. On the other hand, PBO AS averaged crystallite orientation seems to agree reasonably well (Table II). Whilst it is possible that such differences could be attributed to variations in the equipment and fibres used, it is more likely to be attributable to the number of fibres from which the diffraction patterns were taken. When fibre bundles are used, such as in previous studies, any misalignment of fibres in the bundle would result in a decrease in the apparent crystallite orientation. As perfect alignment is practically impossible, this is the most likely source of the difference in orientation. Moreover, instrumental beam broadening should affect the orientation results of Kitagawa *et al*. to a much greater extent compared to those calculated from diffraction patters generated from a synchrotron source. Also differences in the method followed to analyse the diffraction results, i.e., width of the azimuthal slice (Fig. 3b), fitting routine of the intensity profile (Fig. 4), use of integration routines instead of approximation methods [19], can easily render very different absolute $\langle \sin^2 \theta \rangle$ values.

TABLE II Values of initial orientation parameter for the PBO fibre determined using different experimental techniques (ordered by magnitude)

	$\langle \sin^2 \theta \rangle$ TEM [7]	$\langle \sin^2 \theta \rangle$ XRD (bundles) [7]	$\langle \sin^2 \theta \rangle$ XRD (single fibre) [this study]
AS	0.0268	0.0217	0.0189
HM	0.0191	0.0083	0.0028
HM+	0.0161	0.0036	0.0015

When the initial orientation results (Table II) are considered in relation to the fibre tensile properties (Table I), it can be seen that the fibre modulus increases with increasing crystallite orientation, thus the AS fibre has the lowest orientation and modulus, and the HM+ fibre the greatest. It can therefore be concluded that the degree of crystallite orientation is one of the main factors determining the fibre modulus, as has been suggested previously [19, 23, 24]. Indeed, it is this basic assumption which is required when using deformation models such as the aggregate, series-aggregate and continuous chain models [20, 21, 23, 25, 26]. The reason for this orientation-modulus relationship is that increasing orientation increases the influence of direct chain stretching during deformation, and therefore the modulus will increase towards the crystal modulus value, itself an indication of the possible modulus where an applied stress results entirely in chain stretching. For reasons covered in some length in the previous paper, this relationship is however limited by other factors that are significant in reducing the tensile modulus such as density fluctuations and impurities [1].

Importantly however, orientation is also improved by the application of stress, as previously demonstrated by the improvement in orientation following the heat treatment process. This can be observed in Fig. 10 in all three types of fibre. The AS fibre shows the greatest degree of improvement, with the HM and HM+ fibres exhibiting similar crystallite orientation improvement for a given stress level. Upon analysis, it is clear that the degree to which the orientation will improve at a given stress decreases with increasing original orientation parameter ($\langle \sin^2 \theta \rangle_{\sigma=0}$). Thus a fibre with a low orientation such as the AS fibre has a much greater improvement in orientation than a highly orientated fibre such as HM+, for the same level of stress increment. This result agrees with those of other research groups who have also found similar orientation responses to deformation [2, 4, 7]. The degree of improvement in

orientation with deformation was found to be related to the amount of space available for structural change within the fibre [4], with HM+ having the least available and AS the greatest.

The reason for this is that the lower the degree of orientation, the greater the shear forces acting upon the crystallites during the application of stress, and the improvement in orientation is subsequently greater. As the degree of orientation becomes very high, the shear forces required to produce a rotational change in the crystallite angle is similarly much higher, therefore further improvement in orientation is limited.

4. Conclusions

If the crystal strain results are considered first, it can be concluded that there is no discernable difference in crystal strain across the fibre between skin and core with increasing stress, indicating that the fibre deformation is homogenous in this respect. Also, results obtained through the weighted average technique compare favourably with those from the previous paper in this series [1].

The choice of equatorial reflection was found to be significant in measuring skin-to-core orientation differences, and the weighted average results. The (200) reflection was the only reflection to show skin-core differences in orientation parameter, and also returned the lowest overall 'weighted-average' values for all fibre types.

A significant skin-core orientation difference exists only for the AS fibre where the core has a lesser degree of orientation than the skin, attributed possibly to shear forces generated during the spinning process. All three fibres show an increase in the degree of orientation in both skin and core with deformation, although in the AS fibre the orientation of crystallites in the core region improves more than that of the skin. As a consequence, under high levels of deformation there exists little difference between crystallite orientation in the AS fibre skin and core.

The weighted average crystallite orientation results show that the initial level of crystallite orientation increases with increasing fibre modulus for the three PBO fibre types. This initial difference in the degree of orientation between the AS, HM and HM+ fibres can be attributed to differences in their production processes. Orientation is also improved in all three fibres upon the application of stress, the rate of improvement being dependent upon the initial degree of orientation with a lower degree of initial orientation giving the greatest orientation improvement. This can be attributed to the effect of shear forces acting upon the crystallites where, as crystal orientation increases, the forces required for further rotation of the crystallites also increases.

Acknowledgements

The authors would like to extend our thanks to EPSRC for funding this project, the ESRF for beam time, and Toyobo (Japan) for supplying the fibre samples. We would also like to thank Dr. Andrew Hammersley for use of the Fit2D software application, Craig Meakin and all other colleagues in the Manchester Materials Science Centre who have collaborated with us in this work.

References

1. R. J. DAVIES, M. A. MONTES-MORÁN, C. RIEKEL and R. J. YOUNG, *J. Mater. Sci.* **36** (2001) 3079.
2. T. KITAGAWA, M. ISHITOBI and K. YABUKI, *J. Polym. Sci.; Polym. Phys. Ed.* **38** (2000) 1605.
3. P. G. LENHERT and W. W. ADAMS, *Mater. Resear. Soc. Symp. Proc.* **134** (1989) 329.
4. T. KITAGAWA and K. YABUKI, *J. Polym. Sci.; Polym. Phys. Ed.* **38** (2000) 2901.
5. S. J. KRAUSE, T. B. HADDOCK, D. L. VEZIE, P. G. LENHERT, W.-F. HWANG, G. E. PRICE, T. E. HELMINIAK, J. F. O'BRIAN and W. W. ADAMS, *Polymer* **29** (1988) 1354.
6. R. J. YOUNG, R. J. DAY and M. ZAKIKHANI, *J. Mater. Sci.* **25** (1990) 127.
7. T. KITAGAWA, K. YABUKI and R. J. YOUNG, *J. Macromol. Sci.-Phys.* **B41** (2002) 61.
8. T. KITAGAWA, H. MURASE and K. YABUKI, *J. Polym. Sci.; Polym. Phys. Ed.* **36** (1998) 39.
9. M. E. HUNSAKER, G. E. PRICE and S. J. BAI, *Polymer* **33** (1992) 2128.
10. R. J. YOUNG, D. LU, R. J. DAY, W. F. KNOFF and H. A. DAVIS, *J. Mater. Sci.* **27** (1992) 5431.
11. C. RIEKEL, T. DIEING, P. ENGSTROM, L. VINCZE, C. MARTIN and A. MAHENDRASINGAM, *Macromol.* **32** (1999) 7859.
12. R. J. MORGAN, C. O. PRUNEDA and W. J. STEELE, *J. Polym. Sci.; Polym. Phys. Ed.* **21** (1983) 1757.
13. M. G. DOBB and R. M. ROBSON, *J. Mater. Sci.* **25** (1990) 459.
14. D. T. GRUBB, K. PRASAD and W. ADAMS, *Polymer* **32** (1991) 1167.
15. A. V. FRATINI, P. G. LENHERT, T. J. RESCH and W. W. ADAMS, *Mater. Research Soc. Symp. Proc.* **134** (1989) 431.
16. A. P. HAMMERSLEY, ESRF Internal Report, ESRF97HA02T, 'FIT2D: An Introduction and Overview' (1997).
17. P. HAMMERSLEY and C. RIEKEL, *Synchrotron Radiation News* **2** (1989) 24.
18. R. J. YOUNG and P. A. LOVELL, "Introduction to Polymers" 2nd ed. (Chapman & Hall, London, 1991) p. 243.
19. M. G. NORTHOLT, *Polymer* **21** (1980) 1199.
20. M. G. NORTHOLT and J. J. M. BALTUSSEN, *J. Appl. Polym. Sci.* **583** (2002) 508.
21. M. G. NORTHOLT and J. J. VAN AARTSEN, *J. Polym. Sci.; Polym. Symp.* **58** (1977) 283.
22. K. TASHIRO and M. KOBAYASHI, *Macromol.* **24** (1991) 3706.
23. I. M. WARD, *Textile Research Journal* **31** (1961) 650.
24. S. J. KRAUSE, D. L. VEZIE and W. W. ADAMS, *Polym. Commun.* **30** (1989) 11.
25. M. G. NORTHOLT and R. VAN DER HOUT, *Polymer* **26** (1985) 310.
26. W.-Y. YEH and R. J. YOUNG, *ibid.* **40** (1999) 857.

Received 30 July
and accepted 18 December 2002